The Nonnormal Nature of El Niño and Intraseasonal Variability

ANDREW M. MOORE

Program in Atmospheric and Oceanic Sciences, and Cooperative Institute for Research in Environmental Sciences, University of Colorado, Boulder, Colorado

RICHARD KLEEMAN

Bureau of Meteorology Research Centre, Melbourne, Victoria, Australia

(Manuscript received 12 January 1998, in final form 13 October 1998)

ABSTRACT

The idea that intraseasonal variability in the tropical west Pacific can act as an effective means of stochastically forcing ENSO episodes is explored. Using the ideas of generalized linear stability theory as they apply to nonnormal dynamical systems, the physical attributes of the coupled ocean–atmosphere system in the Tropics that allow perturbations with structures that are dissimilar to ENSO to act as precursors for ENSO episodes are examined. Using a coupled ocean–atmosphere model, two particularly important factors are identified that contribute to the nonnormality of the coupled system: nonsolar atmospheric heating directly related to SST changes, and the dissimilarity between the equatorial ocean wave reflection process at eastern and western boundaries. The latter is intrinsic to the dynamics of the ocean, while the former is related to the presence of the west Pacific warm pool and its relationship with the Walker circulation.

1. Introduction

Despite the advances made in developing an understanding of the El Niño Southern Oscillation (ENSO) during the Tropical Ocean Global Atmosphere (TOGA) decade, a debate still rages about the possible nature of El Niño and La Niña precursors. An idea originally proposed in the mid-1980's (Lau 1985; Vallis 1988), that is currently regaining momentum, is that ENSO episodes may be forced by other, essentially stochastic processes in the atmosphere–ocean system (e.g., Penland and Matrasova 1994; Penland and Sardeshmukh 1995; Penland 1996; Kleeman and Moore 1997; Blanke et al. 1997; Eckert and Latif 1997; Kestin et al. 1997; Moore and Kleeman 1999). While there is some compelling observational evidence linking the onset of El Niño episodes to intraseasonal variability in the tropical west Pacific, such as the Madden and Julian Oscillation (MJO), it is not fully appreciated why MJO events occur far more frequently than ENSO events. Recently, Moore and Kleeman (1999) (hereafter MK99) have attempted to explain this apparent disparity in frequency using theoretical ideas relating to stochastic–dynamic systems. In this paper an attempt is made to extend the ideas of MK99 in an effort to answer some fundamental questions about the possible role of intraseasonal variability as a precursor for ENSO episodes, and the possible relationship between the two phenomena. By likening intraseasonal variability to stochastic noise in the coupled system, when viewed on ENSO timescales, MK99 used a stochastically forced, intermediate coupled model (described here in section 3) to answer the question: What would the spatial structure of a stochastic noise forcing have to look like in the tropical Pacific in order for it to increase variability on seasonal-to-interannual timescale associated with ENSO? Figure 1 represents the answer to this question, and shows the surface heat flux and wind stress anomalies that are best suited for enhancing low-frequency variability in a coupled model by exciting ENSO episodes. We will discuss in more detail in section 2 the computations that yield the fields shown in Fig. 1. For now we note that their structure bears a fairly good resemblence to perturbations associated with observed intraseasonal variability and the MJO (see MK99 for a detailed comparison of model results and observations). Furthermore, MK99 show that the coupled model produces very realistic time series of SST variability in response to a stochastic noise forcing composed of structures like those in Fig. 1. MK99 argue that typical perturbations arising from intraseasonal variability have the potential to amplify into mature ENSO episodes, and they discuss in some detail the conditions under which this is likely to occur.

Corresponding author address: Dr. Andrew M. Moore, Program in Atmospheric and Oceanic Sciences, CIRES, University of Colorado, Campus Box 311, Boulder, CO 80309-0311.
E-mail: andy@australis.colorado.edu

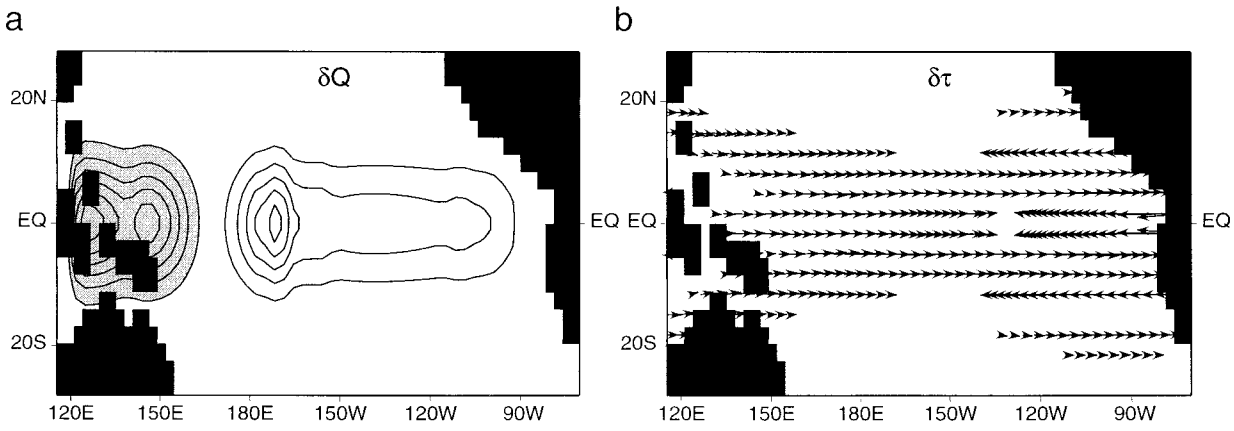

FIG. 1. (a) Contours of surface heat flux, and (b) surface wind stress for the most disruptive stochastic optimal of the Kleeman coupled model. The stochastic optimal is the product of a linear analysis, so the contour interval and vector scales are arbitrary.

It is interesting to note that the 1997–98 El Niño episode fits the mould suggested by MK99. The onset and development of the characteristic El Niño warming of SST in the east Pacific was preceded by two sizable MJO events that produced a clearly observable change in the circulation in the tropical Pacific Ocean. The reader is referred to the TOGA–Tropical Atmosphere Ocean (TAO) Array Web site of Pacific Marine Environmental Laboratory (PMEL) for a detailed observational account of the 1997–98 El Niño (www.pmel.noaa.gov/toga-tao/realtime).

In this paper, we attempt to explain, at least partially, why intraseasonal variability, which has very different time- and space scales to ENSO, may act as a precursor for ENSO episodes. To do this we appeal to some now fairly well-known ideas related to the linear stability of dynamical systems that are summarized in section 2. In sections 3–6 we describe how these ideas can be applied to a simple coupled model that captures rather well the essence of ENSO. The physical factors that most influence the behavior of the system, and which account for the structures shown in Fig. 1 are examined in section 7. An attempt is made in section 8 to relate ENSO and the MJO to the Walker circulation and seasonal cycle. A summary of our results and conclusions can be found in section 9.

2. Linear theory

The ideas presented in this section are fairly well known and are discussed in detail elsewhere (e.g., Farrell and Ioannou 1996a,b), so we will state only the results that are relevant to this study. We will represent by Ψ the state vector that describes the coupled ocean–atmosphere system in the Tropics, and assume that Ψ is governed by the nonlinear equation:

$$\frac{\partial \Psi}{\partial t} = L(\Psi). \tag{1}$$

Small perturbations ψ to Ψ evolve according to the so-called tangent linear equation arising from a first-order Taylor expansion of (1):

$$\frac{\partial \psi}{\partial t} = \left(\frac{\partial L}{\partial \Psi}\right)\psi. \tag{2}$$

Over the time interval $t = t_1 \rightarrow t_2$, we have:

$$\psi(t_2) = R(t_1, t_2)\psi(t_1), \tag{3}$$

where $R(t_1, t_2)$ is the linear propagator of the system. According to (2) we have:

$$R(t_1, t_2) = \exp\left(\int_{t_1}^{t_2} \frac{\partial L}{\partial \Psi}\, dt\right). \tag{4}$$

For the autonomous case Ψ is stationary in time so (4) becomes:

$$R(t_1, t_2) = \exp\left(\frac{\partial L}{\partial \Psi}(t_2 - t_1)\right). \tag{5}$$

The eigenvectors of R in this case are the so-called normal modes of the coupled system. For the nonautonomous case, $\Psi = \Psi(t)$ and $R(t_1, t_2)$ is given by (4). The eigenvectors of R in this case are the so-called ''finite-time normal modes'' of the coupled system.

We will denote by $R^\dagger$ the adjoint of R where

$$\langle \psi^\dagger, R\psi \rangle = \langle R^\dagger \psi^\dagger, \psi \rangle \tag{6}$$

and where ψ and $\psi^\dagger$ are arbitrary perturbations, and $\langle \ldots, \ldots \rangle$ denotes an inner product. If we denote by η_i the eigenvectors of R, and by $\eta_j^\dagger$ the eigenvectors of $R^\dagger$, then we have:

$$\langle \eta_i, \eta_j^\dagger \rangle = \delta_{i,j} \tag{7}$$

for suitably normalized eigenvectors. From (6) and (7) we can show that $\eta_k^\dagger$ is the optimal excitation for η_k in the tangent linear model (2) (Farrell 1989). For an autonomous system we will refer to η_i as the normal modes

and for a nonautonomous system as the finite-time normal modes. Similarly we will refer to $\eta_j^\dagger$ as the adjoint normal modes or adjoint finite-time normal modes.

In general, it is more convenient to work with discrete forms of (1) and (2), so we will denote by $\mathbf{R}$ the discrete form of the propagator R, in which case $\mathbf{R}^{\mathrm{T}} \equiv R^\dagger$. Now, in general, for linear dynamical operators or matrices for which $\mathbf{R}^{\mathrm{T}}\mathbf{R} = \mathbf{R}\mathbf{R}^{\mathrm{T}}$ the system is said to be normal. In this case, the eigenvectors of $\mathbf{R}$ and $\mathbf{R}^{\mathrm{T}}$ are identical and form orthogonal sets. On the other hand, if $\mathbf{R}^{\mathrm{T}}\mathbf{R} \neq \mathbf{R}\mathbf{R}^{\mathrm{T}}$ then the dynamical system is said to be nonnormal. In this case the eigenvectors of $\mathbf{R}$ and $\mathbf{R}^{\mathrm{T}}$ are different and nonorthogonal, but obey the biorthogonality relation (7).

Also of interest are the singular vectors of $\mathbf{R}$, which by definition are the eigenvectors of $\mathbf{R}^{\mathrm{T}}\mathbf{R}$. These are the fastest growing perturbations that can exist in the system described by (1) before nonlinearity becomes important. For this reason the singular vectors are often referred to as optimal perturbations.

If the system described by (1) and (2) is subject to a noise forcing that is white in time, then an additional set of eigenvectors are of interest, namely those of the matrix $\mathbf{Z}$ given by:

$$\mathbf{Z} = \int_0^\tau \mathbf{R}^{\mathrm{T}}\mathbf{R}\, dt. \tag{8}$$

The eigenvectors of $\mathbf{Z}$ with largest eigenvalues are sometimes called forcing orthogonal functions (Farrell and Ioannou 1993) or stochastic optimals (Kleeman and Moore 1997), and represent the patterns of surface noise forcing that are most disruptive to the system.

3. Application of linear theory to the tropical coupled ocean–atmosphere system

The ideas presented in section 2 form the basis of generalized linear stability theory. When applied to models of the coupled ocean–atmosphere system in the Tropics, the normal mode η_0 with the largest eigenvalue often describes a model's representation of ENSO. Perhaps more generally we should say that η_0 describes variability on seasonal-to-interannual timescales in such models.

The ideas described in section 2 have been applied in a series of papers by Moore and Kleeman (1996, 1997a,b, 1998, 1999) and Kleeman and Moore (1997, 1999) to a coupled model of ENSO, hereafter referred to as the Kleeman model. Moore and Kleeman (1997b) have found that a normal mode exists in the Kleeman model that describes the model's ENSO. They also found that the optimal perturbations (Moore and Kleeman 1997a,b) and stochastic optimals (Kleeman and Moore 1997) of the Kleeman model bear a remarkable resemblence to structures observed in nature, such as westerly wind bursts, that are associated with intraseasonal variability in the tropical west Pacific. Furthermore, a stochastic noise forcing composed of perturbations with these structures can produce SST variability in the NINO3 region with variability on seasonal-to-interannual timescales that is remarkably like that observed (MK99).

The structure of ENSO is quite different to that of intraseasonal variability. The reason why ENSO can be excited by perturbations with structures that are very different to the structure of ENSO is due to the nonnormal nature of the coupled ocean–atmosphere system as described in section 2. We will demonstrate that the normal mode describing ENSO and its adjoint, which is an optimal excitation for the normal mode, have very different structures in the Kleeman model due to the nonnormal nature of the dynamics that describe interannual variability in the coupled system.

Based on their findings, MK99 have proposed that intraseasonal variability, such as the MJO and westerly and easterly wind bursts, can act as an effective stochastic forcing mechanism for ENSO, and if true this has tremendous ramifications for ENSO prediction and predictability. If this is true, then it is pertinent to ask why intraseasonal variability creates disturbances in the western tropical Pacific with structures that appear to be optimal for exciting ENSO? Is there a merely coincidental match between the structures of MJO-induced perturbations and the optimal excitation for ENSO, or are the two phenomena dynamically linked in some way by the large-scale general circulation? We will attempt to address this question using the ideas described in section 2.

4. The Kleeman coupled model

The Kleeman model is an intermediate coupled model of the tropical Pacific Ocean and global atmosphere (Kleeman 1993) and computes anomalies about the time varying climatological seasonal cycle, which is prescribed from observations. The coupled model is used operationally at the Bureau of Meteorology Research Centre (BMRC) for seasonal forecasting (Kleeman 1994). Full details of the model equations and solution techniques can be found in Kleeman (1989, 1993), so we present only a brief description of the model here.

The atmospheric component of the model is a linear, two-level, damped, steady-state, Gill model that describes the first baroclinic mode circulation of the tropical atmosphere. The atmospheric model describes the anomalous circulation at 750 mb about the observed time varying seasonal cycle, which is prescribed (Kleeman 1991). The atmosphere is heated in two ways: (i) by direct thermal forcing (DTF) that is directly proportional to SST anomalies, and represents the effects of sensible heating, shallow convection, and radiation that are not explicitly modeled, resolved, or parameterized in the model; and (ii) by latent heating (LH) due to deep penetrative convection in the atmosphere. DTF and LH are parameterized as follows:

$$\mathrm{DTF} = \epsilon_a \mathcal{R} T / 2c_a^2, \tag{9}$$

$$\begin{aligned}\mathrm{LH} = \mathcal{R}/2c_a^2\langle (I_1\{|\mathbf{U}|[q_{\mathrm{diff}}(\overline{T}+T)] \\ + |\overline{\mathbf{U}}|[q_{\mathrm{diff}}(\overline{T}+T) - q_{\mathrm{diff}}(\overline{T})]\} \\ + I_2[(\overline{q}+q)\boldsymbol{\nabla}\cdot\mathbf{U} + q\boldsymbol{\nabla}\cdot\overline{\mathbf{U}} \\ + (\overline{\mathbf{U}}+\mathbf{U})\cdot\boldsymbol{\nabla}q + \mathbf{U}\cdot\boldsymbol{\nabla}\overline{q}])\rangle,\end{aligned} \tag{10}$$

where T is the SST anomaly, $\mathbf{U}$ is the wind anomaly, $q_{\mathrm{diff}}(\mathcal{T})$ is the air–sea specific humidity difference at temperature $\mathcal{T}$, q is the specific humidity, $\mathcal{R}$ is the gas constant for dry air, ϵ_a is a Newtonian cooling coefficient, and c_a^2 is the first baroclinic mode phase speed for the atmosphere. An overbar denotes observed seasonally varying mean quantities, while all other quantities represent anomalies. Equation (10) results from integrating the atmospheric moisture equation vertically, and I_1 and I_2 incorporate the constants of integration and various other physical constants (i.e., the latent heat of evaporation, the latent heat exchange coefficient, the specific heat capacity of air, and air density). The first term in (10) in $\{\ldots\}$ represents latent heat release from the ocean surface due to convectively induced surface wind anomalies, while the second term in $[\ldots]$ represents latent heat release due to moisture convergence in the atmosphere. In accordance with observations, LH occurs only when the total SST (i.e., climatological SST for a given day + SST anomaly) exceeds about 28°C (Graham and Barnett 1987).

The ocean component of the Kleeman model describes the dynamics of the first baroclinic mode subject to the equatorial long wave approximation. The equatorial SST anomaly T evolves according to:

$$\partial T/\partial t - \alpha h + \epsilon T = 0, \tag{11}$$

where h is the ocean thermocline depth anomaly, α is a constant of proportionality that varies with longitude, and ϵ is a Newtonian cooling coeffient. Equation (11) describes the fact that vertical movements of the thermocline can create SST anomalies in the presence of equatorial upwelling along the equator. Different values are used for α in the west and east Pacific to reflect the fact that (a) the main thermocline is deeper in the west than the east, and (b) in general the rate of oceanic upwelling is large in the east and central Pacific and very weak in the west Pacific. In the east Pacific from the coast of Central America to 140°W, $\alpha = \alpha_E = 3.4 \times 10^{-8}$ °C m^{-1} s^{-1}, while in the west Pacific, $\alpha = \alpha_W = \alpha_E/5$. In the central Pacific between 140°W and the date line, α varies linearly between α_E and α_W. Steady-state solutions of (11) yield $T = 2$°C when $h = 15$ m. Here α can also vary seasonally in accordance with the seasonal cycle in mean upwelling. Horizontal advection can also influence the development of SST anomalies. We will discuss this mechanism in section 7c, but for now we confine our attention to the case described by (11).

In section 5 we will discuss the ability of the coupled model to support self-sustaining or damped oscillations, which depends on the following model parameters: the phase speed of equatorial Kelvin waves in the ocean, c_o, and atmosphere, c_a; the coupling strength between the ocean and atmosphere γ, which enters as a mean wind speed in the linear drag law used to compute surface wind stress anomalies; the Newtonian cooling coefficients ϵ_a and ϵ; and the parameter α in (11). When run operationally at BMRC, with $c_o = 2.8$ m s^{-1}, $c_a = 60$ m s^{-1}, $\gamma = 7$ m s^{-1}, $\epsilon_a = (3 \text{ days})^{-1}$, and α as given above, the coupled model produces a damped oscillation with a period of approximately 3 yr with characteristics similar to those of the observed ENSO. Figure 2 shows Hovmöller diagrams of T and h along the equator. Using

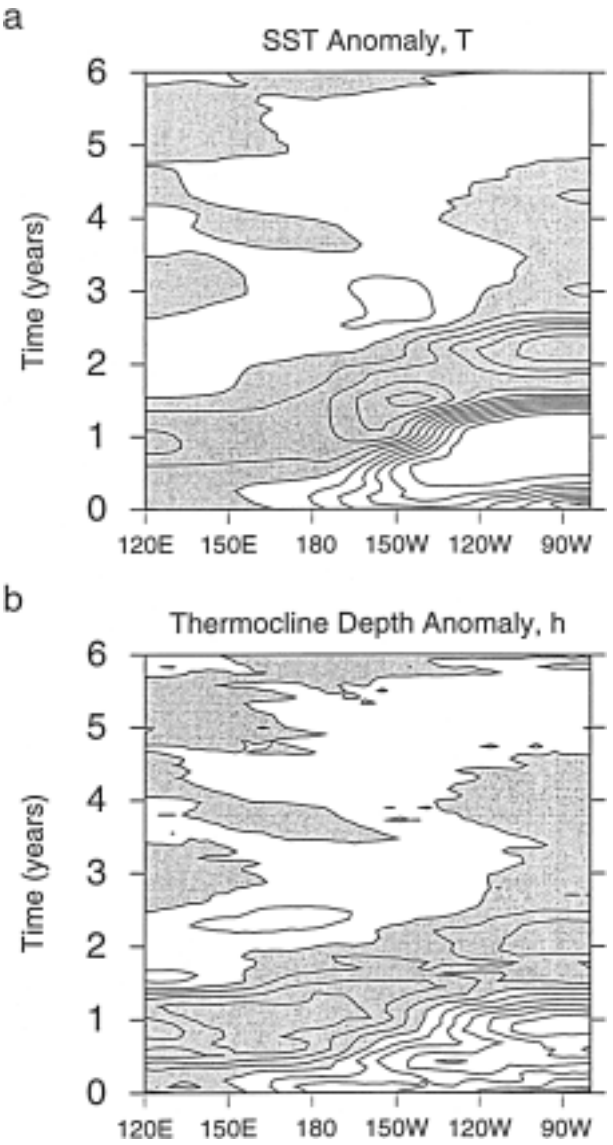

FIG. 2. Hovmöller diagrams of SST anomaly T and thermocline depth anomaly h along the equator from the nonlinear Kleeman coupled model. The contour interval for SST is 0.5°C and 10 m for h. Shaded regions represent negative anomalies.

principal oscillation pattern (POP) analysis, Kleeman and Moore (1999) have shown that the POP describing ENSO in the Kleeman model is very similar to the ENSO POP computed from observations.

The Kleeman model possesses two very important and physically realistic nonlinearities. The first relates to the latent heating due to deep penetrative convective anomalies described by LH in (10). As noted LH differs from zero only when the moist static energy of air parcels exceeds a critical value corresponding to an SST of approximately 28°C. The second nonlinearity relates to the effect of thermocline depth anomalies h on SST described by (11). When the thermocline is very deep or very shallow, further changes in depth of the thermocline do not influence SST. Despite the presence of these nonlinearities, we can apply the linear ideas of section 2 to the Kleeman model by linearizing about a background state that includes the effects of nonlinearity. Details of the linearization can be found in Moore and Kleeman (1996, 1997a).

5. The normal mode spectrum of the Kleeman model

If the coupled model is linearized about the observed annual mean climatological state of the coupled system, then the resulting tangent linear equations describe an autonomous system, and $\mathbf{R}$ is given by (5). The normal modes of the Kleeman model can therefore be found by computing the eigenvectors of the autonomous linear operator $\mathbf{R}$. As the parameters c_o, α, γ, c_a, ϵ, etc., are varied the stability of the coupled system changes as the primary bifurcation point is approached (Kleeman 1993; Moore and Kleeman 1997b). Probably the most important factor governing the stability of the system is the ocean–atmosphere coupling strength γ.

Figures 3a and 3b show the period T_i and e-folding decay time D_i for the first eight members ($i = 0 \rightarrow 7$) of the normal mode spectrum of the coupled model. In this case a value of $\gamma = 11$ m s^{-1} is chosen so that the model is stable, but close to its primary bifurcation point. The normal mode with the lowest frequency has a period of $T_0 = 36$ months, and an e-folding decay time $D_0 = 48$ months. The remaining modes have progressively higher frequencies but interestingly all have the same e-folding decay time, $D_i = 16$ months, $i = 1 \rightarrow 7$. The factor by which any quadratic norm of a given mode decays over the time period τ is given by $e^{-2\tau/D_i}$. Therefore modes 1–7 all have the same decay factors for any quadratic norm. Figure 3b shows that the least damped mode (i.e., the ''gravest mode,'' $i = 0$) decays three times more slowly than the other modes.

The least damped normal mode in Figs. 3a and 3b has a structure that is very similar to the model ENSO as we will show in section 6. Therefore, to distinguish it from all the other normal modes we will refer to this mode as the ''ENSO mode.'' The period T_0 of the ''ENSO mode'' is relatively insensitive to the value of γ, and the distribution of points in Fig. 3a changes little as γ is varied on both sides of the bifurcation point. The e-folding decay time D_0 of the ENSO mode, however, decreases rapidly with decreasing γ, and approaches a value of 16 months. This behavior is also reminiscent of the coupled modes studied by Hirst (1986) for a system similar to that considered here. For all values of γ investigated, the ENSO mode is always present within the normal mode spectrum.

When the Kleeman model is subject to stochastic forcing reminiscent of observed intraseasonal variability, MK99 demonstrate that the most realistic spectra of seasonal-to-interannual variability arise when the system is stable but close to the primary bifurcation point. On the other hand, Blanke et al. (1997) and Eckert and Latif (1997) have argued more in favor of a stochastically forced unstable coupled system. In either case, the ideas and results that are presented here apply to both stable and unstable systems.

6. Normal modes of the coupled model

The least damped normal mode (for a stable system) or most unstable normal mode (for an unstable system) of the tangent linear Kleeman model strongly resembles the damped oscillation shown in Fig. 2. Using the notation of section 2 we will denote this mode as η_0, and the linear theory of section 2 allows us to identify the model ENSO as η_0.

The typical structure of the ENSO mode perturbation SST, δT, and thermocline depth perturbation, δh, is shown in Fig. 4. Like the damped ENSO oscillation of the nonlinear model (see Fig. 2) the structure of the ENSO mode in Fig. 4 agrees well with the POP analysis of observed tropical interannual variability in the Pacific (Kleeman and Moore 1999). The ENSO mode has its largest SST amplitude in the east Pacific. Variations in γ produce only minor variations in the frequency and structure of this mode. The main effect of nonlinearity on the ENSO mode is the introduction of a modest asymmetry in the duration of the warm and cold phases of the ENSO oscillation. The period and propagation characteristics of the model ENSO are very similar in the linear and nonlinear models.

The adjoint ENSO mode $\eta_0^\dagger$ for the same system is shown in Fig. 5. In constrast to η_0, the adjoint ENSO mode $\eta_0^\dagger$ has its largest amplitude confined primarily in the central and west Pacific. The SST structure of $\eta_0^\dagger$ is very similar to that of the stochastic optimal heat flux of the coupled model shown in Fig. 1a, and consists of an SST dipole over the west Pacific. We recall from section 2 that $\eta_0^\dagger$ represents the optimal excitation for η_0 in the tangent linear model. The eigenvalues of $\mathbf{R}$ and $\mathbf{R}^{\mathrm{T}}$ are identical so the frequency and growth/decay rates of the adjoint modes are identical to those in Figs. 3a and 3b. If the tangent linear model is initialized with $\eta_0^\dagger$, the SST dipole in the west produces a coherent patch of westerly or easterly winds spanning the equator de-

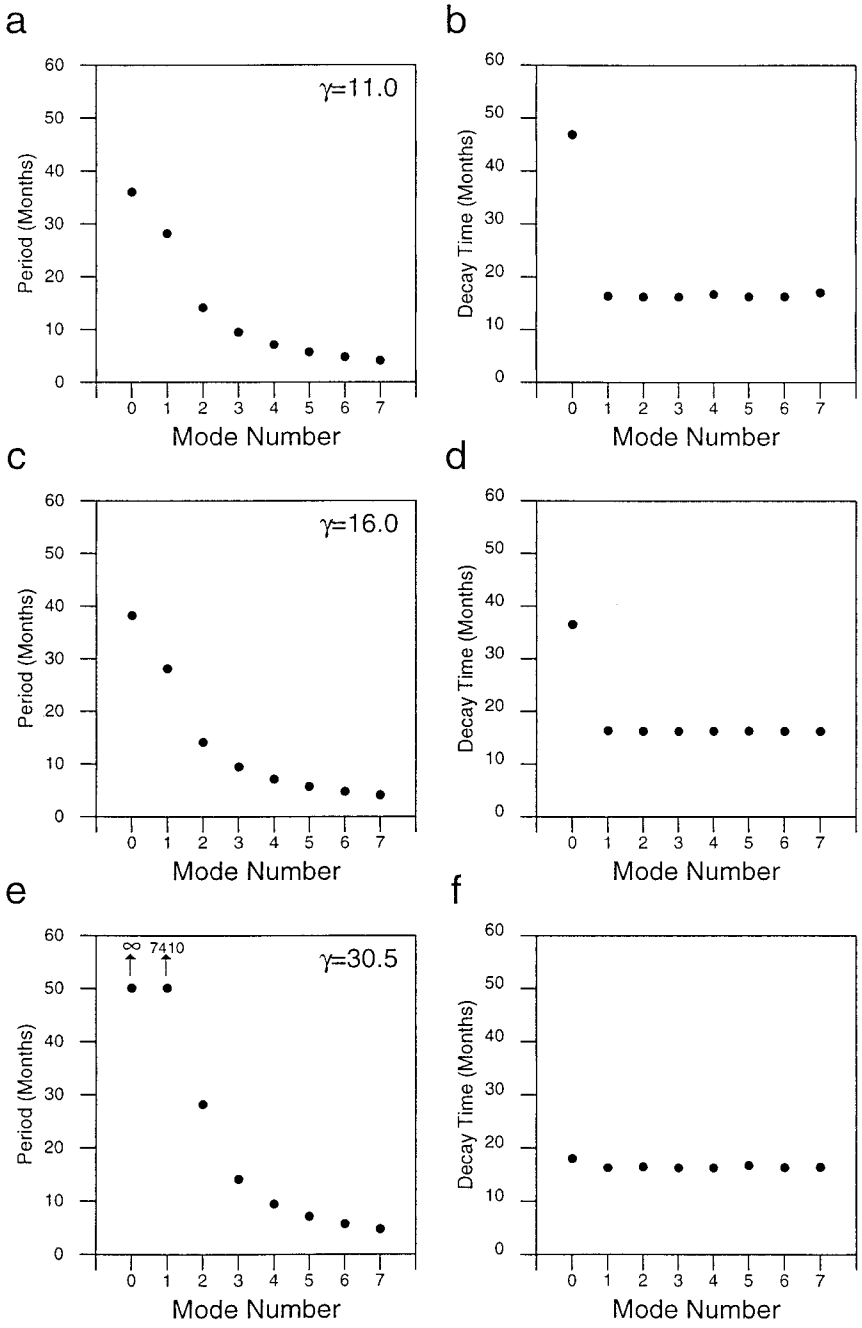

FIG. 3. (a) The period and (b) *e*-folding decay time of the first eight members of the normal mode spectrum of the tangent linear coupled model. (c, d) Same as (a, b) except that $\delta\mathrm{LH} = 0$. (e, f) Same as (a, b) except that $\delta\mathrm{DTF} = 0$.

pending on the sign of $\eta_0^\dagger$, and an ENSO episode rapidly develops as η_0 emerges. Figure 6 shows time series of $\ln[N(t)]$, where $N(t) = \mathrm{SST}^2(t)/\mathrm{SST}^2(0)$, and $\mathrm{SST}^2(t)$ is the zonal integral of δT^2 along the equator. Two cases are shown: one when the tangent linear coupled model is initialized with a perturbation that is a snapshot of the structure of η_0, and one when the same model is initialized with a perturbation that is a snapshot of the structure of $\eta_0^\dagger$. The model is stable with $\gamma = 11$ m s^{-1} but close to the primary bifurcation point. In both cases the ENSO mode η_0 emerges in the model, but when the adjoint ENSO mode is used the amplitude of η_0 is three times larger than when the ENSO mode itself is used. This chain of events is very similar to that described by Moore and Kleeman (1996, 1999) as a result of optimal perturbations or stochastic optimal forcing with

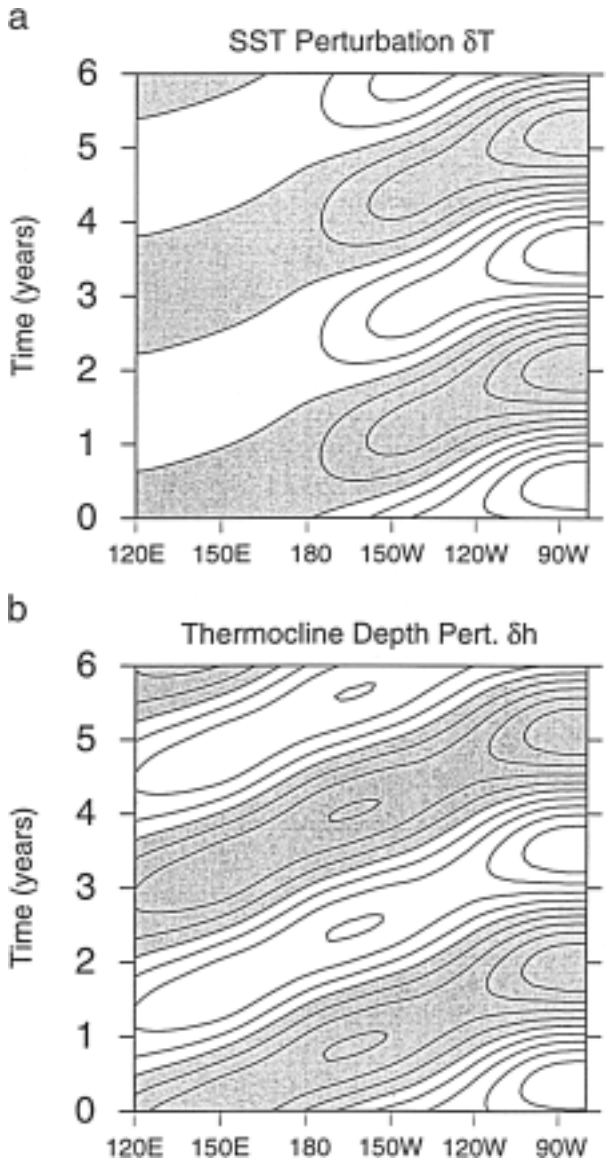

FIG. 4. Hovmöller diagrams of SST perturbation δT and thermocline depth perturbation δh along the equator for the gravest normal mode of the tangent linear coupled model. This mode is hereafter referred to as the ''ENSO mode.'' Because the normal mode is a solution of the tangent linear model, the contour intervals are arbitrary. Shaded regions represent negative perturbations.

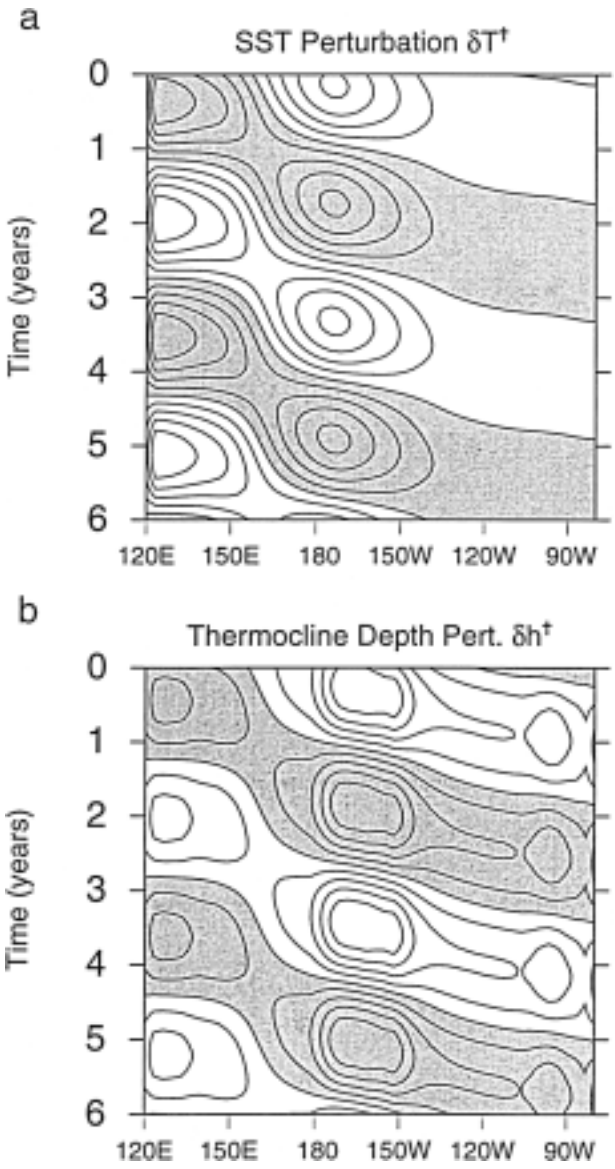

FIG. 5. Hovmöller diagrams of the adjoint SST perturbation $\delta T^{\dagger}$ and adjoint thermocline depth perturbation $\delta h^{\dagger}$ along the equator for the gravest adjoint normal mode. This mode is hereafter referred to as the ''adjoint ENSO mode.'' Because the adjoint normal mode is a solution of the adjoint tangent linear model, the contour intervals are arbitrary. Shaded regions represent negative perturbations. The time axis is reversed because the adjoint model is run backward in time.

spatial structures that resemble observed intraseasonal variability. Large-scale surface heat flux anomalies with spatial structures similar to the SST structure of $\eta_0^{\dagger}$ often occur in nature associated with intraseasonal variability. So if we believe that the Kleeman model captures the dynamics important for ENSO, Fig. 5 indicates that SST perturbations arising from intraseasonal variability such as the MJO could act as effective precursors for ENSO episodes.

To understand how this situation arises, it is necessary to understand why the structures of the ENSO mode η_0 and adjoint ENSO mode $\eta_0^{\dagger}$ in Figs. 4 and 5 are different. As noted in section 2, this is related to the nonnormal nature of the coupled system in which the normal modes are nonorthogonal. As a consequence of this we can ''hide'' the structure of η_0 by a linear superposition of the other more rapidly damped normal modes (or more slowly growing or neutral modes depending on the value of γ). As this superposition of modes evolves in time, η_0 quickly emerges. The adjoint ENSO mode $\eta_0^{\dagger}$ is the optimal combination of normal modes that works best for ''hiding'' a large amplitude η_0 as demonstrated in

Fig. 6. Therefore, developing an understanding of the physical factors that contribute to the nonnormality of the coupled system will help us to understand why ENSO (described by η_0) can be effectively excited by intraseasonal variability that produces perturbations with spatial structures that project heavily onto snapshots of $\eta_0^\dagger$.

7. Factors that influence the nonnormality of the coupled system

To understand the dynamical factors that influence the nonnormality of the coupled system it is necessary to identify the physical processes that render the propagator R in (4) nonnormal. Following the notation introduced in section 2, we denote by Ψ the state vector of the coupled ocean–atmosphere system such that $\Psi = (\mathbf{M}, \mathbf{O})$ where $\mathbf{M}$ and $\mathbf{O}$ are the state vectors of the atmosphere and ocean, respectively. Following section 2, we denote by ψ a small perturbation to Ψ. The tangent linear equation for the coupled model can then be expressed symbolically as:

$$\frac{\partial \psi}{\partial t} + \underbrace{\begin{pmatrix} \underline{D_a} & CT_a & PG_a & 0 & 0 & 0 & 0 \\ CT_a & \underline{D_a} & PG_a & 0 & 0 & 0 & 0 \\ Div_a & Div_a & \underline{D_a} & \underline{AH} & 0 & 0 & 0 \\ 0 & 0 & 0 & \underline{D_o} & 0 & 0 & \underline{OT} \\ \underline{WS} & 0 & 0 & 0 & \underline{D_o} & CT_o & PG_o \\ 0 & \underline{WS} & 0 & 0 & CT_o & 0 & PG_o \\ 0 & 0 & 0 & 0 & Div_o & Div_o & \underline{D_o} \end{pmatrix}}_{\mathbf{A}} \psi = 0, \tag{12}$$

where D represents dissipation (Rayleigh friction or Newtonian cooling), CT is a Coriolis acceleration, PG is a pressure gradient acceleration, Div is horizontal divergence, AH = δDTF + δLH represents atmospheric heating where δ denotes the tangent linear forms of (9) and (10), WS is the perturbation surface wind stress, and OT represents ocean thermodynamics that control SST perturbations given by the tangent linear form of (11). The subscripts a and o refer to atmospheric and oceanic terms, respectively.

The mathematical form of PG_a and Div_a are identical, as are PG_o and Div_o. The underscored terms in (12) change sign when the adjoint $\mathbf{A}^\dagger$ of $\mathbf{A}$ is computed, and represent the physical processes that contribute to the asymmetry and nonnormal nature of the dynamical operators that govern the linear development of perturbations in the coupled model. These terms correspond to:

1) dissipation, D;
2) the influence of upper-ocean thermodynamics (OT) on SST described by the tangent linear form of (11);
3) the direct thermal forcing δDTF and latent heating δLH in the troposphere described by the tangent linear forms of (9) and (10);
4) the surface perturbation wind stress, WS;
5) the asymmetry of the reflection properties of equatorial ocean waves at east and west boundaries.

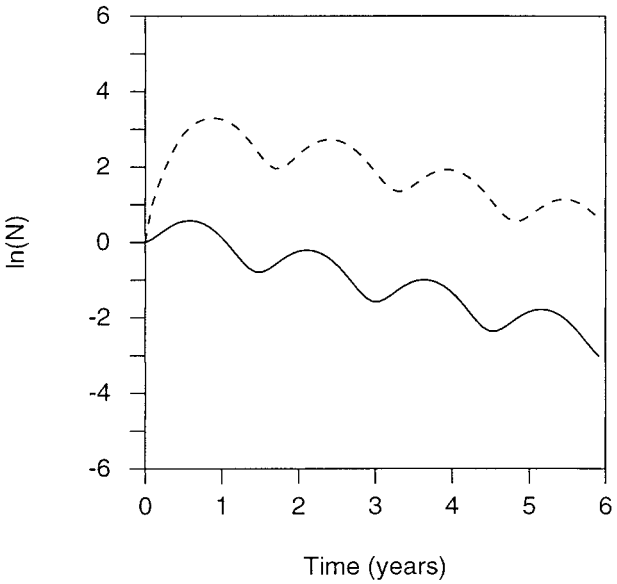

FIG. 6. Times series of ln(N) when the tangent linear coupled model is initialized with a snapshot of the ENSO mode (solid curve), and when initialized with a snapshot of the adjoint ENSO mode (dashed curve). In this case $\gamma = 11$ m s^{-1}.

In nature, or in a more complex model, there will be other factors such as interactions between the atmosphere and biosphere that also render the system nonnormal.

A physical mechanism that renders the coupled system nonnormal is one that operates in only one direction. For example, the surface wind stress drives a flow in the ocean through the action of turbulent stresses in the upper-ocean mixed layer. Thus if the atmosphere is in motion, the ocean will be set in motion. However, surface currents in the ocean do not exert a significant drag on the atmosphere above, meaning that frictional drag between the ocean and atmosphere is not a means of setting the atmosphere in motion, hence there are no terms in (12) proportional to the ocean surface currents that act to accelerate the atmosphere. Therefore this form of communication between the atmosphere and the ocean is a ''one-way street.'' Similar arguments can be applied to factors (1)–(3). Suppose for a moment that the ''one-way streets'' of (1)–(5) became ''two-way streets,'' then it is easy to see that the additional physical interactions that would be added to the system could render the system normal.

Nonnormality in the atmosphere and ocean is more usually linked to the presence of shear and strain in the basic-state flow. Factors (1)–(5) show that physical fac-

tors other than shear and strain can influence the nonnormality of the coupled system.

Factor (5) becomes apparent only when we consider the boundary conditions that must be applied to $\psi^\dagger$ to render zero the boundary integrals arising from the integration by parts implied by (6). Computation of the adjoint boundary conditions (not shown) indicates that an adjoint Kelvin wave propagates westward and is initiated at an eastern boundary by adjoint planetary wave reflections. Adjoint Kelvin waves give up energy to adjoint planetary waves at a western boundary that propagate eastward. The opposite phase velocities of equatorial ocean waves compared to their adjoint counterparts is a consequence of the fact that the adjoint of equation (12) must be integrated backward in time to render zero the boundary terms that involve the initial conditions of the tangent linear coupled system and the final conditions of the adjoint coupled model (see Lanczos 1961). It is the asymmetry of the wave reflections at the eastern and western boundaries and the opposite directions of the group velocities of equatorial Kelvin waves and long planetary waves that is partly responsible for the confinement of the ENSO normal mode SST pattern to the east Pacific.

Clearly the five factors listed above are responsible for the nonnormal nature of the coupled ocean–atmosphere system in the Tropics. Our interest now lies in which of these factors (or combination of them) is primarily responsible for the dipole structure of the adjoint ENSO mode in Fig. 5 on which intraseasonal variability may project and excite the ENSO mode. This aspect of the coupled system was investigated by comparing the normal modes and adjoint normal modes that result by varying the model parameters that control factors (1)–(4). Factor (5) is instrinsic to the dynamics of the equatorial ocean circulation so we cannot modify this without fundamentally altering the physics of the ocean circulation.

a. Variations in mode structure with atmospheric heating

In this section we will examine the influence of atmospheric heating [AH in (12)] on the normal mode structures. For convenience we will refer to the model with both direct thermal forcing δDTF and latent heating δLH as the ''full'' tangent linear model. We begin by examining the normal modes when $\delta\text{DTF} \neq 0$ and $\delta\text{LH} = 0$, so that only perturbations in DTF influence the atmosphere. Figures 3c and 3d show the periods T_i and e-folding decay times D_i for $i = 0 \rightarrow 7$ at a stable point close to the primary bifurcation when $\delta\text{LH} = 0$. Note that for a particular value of γ, choosing $\delta\text{LH} = 0$ renders the coupled system more stable compared to the full model. When $\delta\text{LH} = 0$, the primary bifurcation point lies close to $\gamma = 16$ m s^{-1}, compared to $\gamma = 11$ m s^{-1} for the full model. Comparing Figs. 3c and 3d with Figs. 3a and 3b shows that the shape of the spectra is affected little by the absence of δLH, and in each case the ENSO mode with $T_0 = 36$ months is present, and is the least damped mode.

Figures 7a and 7b show the structure of δT and δh for the gravest normal mode, η_0, when $\delta\text{DTF} \neq 0$ and $\delta\text{LH} = 0$. The normal mode oscillates with a period similar to that of η_0 for the full tangent linear model. The character of the thermocline depth anomalies of η_0 are changed somewhat from eastward propagating to a predominantly standing wave pattern when $\delta\text{LH} = 0$, but the SST structure is similar in both cases.

Consider now the case where the direct thermal forcing term $\delta\text{DTF} = 0$ and $\delta\text{LH} \neq 0$. The periods T_i and decay times D_i for $i = 0 \rightarrow 7$ are shown in Figs. 3e and 3f for this case for $\gamma = 30.5$ m s^{-1}, which is close to the primary bifurcation of this system. This value of γ is almost three times larger than that where the full model becomes unstable, so δDTF has a large influence on the stability of the coupled model. Figure 3e shows that the least damped mode is stationary, and in fact there is no normal mode corresponding to the ENSO mode in this case. The gravest normal mode for this case is shown in Figs. 7c and 7d and has its largest amplitude in the west Pacific.

Figure 7 indicates that the oscillatory character of the ENSO mode in Fig. 4 is due to δDTF. If $\delta\text{LH} = 0$, Figs. 7a and 7b show that the structure of the resulting normal mode is very similar to that of Fig. 4 indicating that the main role played by δLH is to reduce the stability of the ENSO mode, while having a modest influence on its structure.

The gravest adjoint normal mode when $\delta\text{LH} = 0$ and $\delta\text{DTF} \neq 0$ is shown in Figs. 8a and 8b, which corresponds to the optimal excitation for the normal mode of Figs. 7a and 7b. With $\delta\text{LH} = 0$ the adjoint normal mode has a very different SST structure to the adjoint ENSO mode of the full model shown in Fig. 5. When $\delta\text{LH} = 0$, the adjoint mode has a large amplitude over the west, central, and eastern Pacific, and the SST patterns of η_0 and $\eta_0^\dagger$ in the central and east Pacific in Figs. 7a and 8a show some similarities.

The gravest adjoint normal mode $\eta_0^\dagger$ when $\delta\text{DTF} = 0$ and $\delta\text{LH} \neq 0$ is shown in Figs. 8c and 8d. Like its counterpart normal mode (cf. Figs. 7c and 7d) it is stationary and nonoscillatory with largest amplitude in the west.

A comparison of Figs. 8a,b and 5 indicates that the δLH atmospheric heating term plays a greater role in shaping the structure of the gravest adjoint normal mode than it does for the gravest normal mode (cf. Figs. 7a,b with Fig. 4). When $\delta\text{LH} = 0$ the adjoint normal mode SST pattern is spread across the entire tropical Pacific, but when $\delta\text{LH} \neq 0$ the adjoint mode SST signature is confined to the west Pacific.

1) ENSO MODE DYNAMICS

The influence of δDTF and δLH on the gravest normal mode and adjoint normal mode can be understood

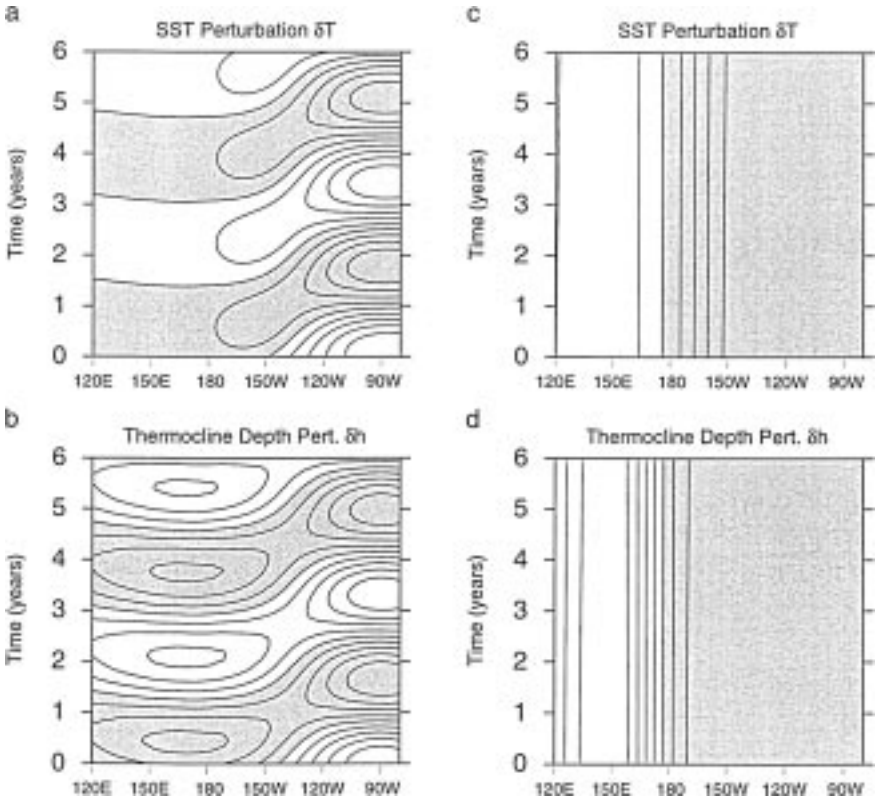

FIG. 7. Hovmöller diagrams of (a) SST perturbation δT and (b) thermocline depth perturbation δh along the equator for the gravest normal mode of the tangent linear coupled model when δDTF $\neq 0$ and δLH $= 0$. Hovmöller diagrams of (c) δT and (d) δh for the gravest normal mode when δDTF $= 0$ and δLH $\neq 0$ are also shown. The contour intervals are arbitrary. Shaded regions represent negative perturbations.

if we consider the dynamics of the modes and the spatial structure of the these two atmospheric heat sources. In the model, SST can change only by vertical movements of the ocean thermocline according to (11). Consider an equatorial Kelvin wave in the west Pacific moving eastward and deepening the thermocline. In the west Pacific the mean depth of the ocean thermocline is deep and there is no appreciable upwelling, so changes in depth of the ocean thermocline do not have much influence on SST in the west Pacific. This is reflected in the coupled model by a small value of α in the west Pacific in (11). As a result δDTF is small in the west Pacific since δT due to the passage of the Kelvin wave is small. As the Kelvin moves into the central and east Pacific where the thermocline is shallow and upwelling strong, large SST anomalies can develop there. This is reflected in the coupled model with α in (11) increasing eastward. As a result large SST perturbations δT can develop, hence δDTF is much larger in the east Pacific than it is in the central and west Pacific. As δDTF increases, the ocean and atmosphere become more strongly coupled and a coupled Kelvin wave develops, which accounts for the structure of the dominant ENSO mode in Figs. 2 and 4 (Hirst 1986; Kleeman 1993). Therefore, equatorial ocean Kelvin dynamics in association with zonal variations in the mean depth of the ocean thermocline and rate of equatorial upwelling (reflected in α) essentially confine the influence of δDTF to the east Pacific. Equatorial planetary waves do not play a significant role in directly controlling SST near the equator since they have their largest influence on h off the equator outside of the regions of strong equatorial upwelling.

2) ADJOINT ENSO MODE DYNAMICS

Consider now the latent heating described by δLH. This is nonzero only when the basic-state SST is greater than about 28°C. Therefore δLH is confined to the region occupied by the west Pacific warm pool. Since the gravest coupled normal mode η_0 of the full tangent linear model that describes the model ENSO is primarily controlled by equatorial ocean Kelvin wave dynamics, the adjoint ENSO normal mode $\eta_0^\dagger$ is controlled by adjoint Kelvin wave dynamics. So consider now the case of an adjoint equatorial Kelvin wave in the adjoint coupled model. By convention the adjoint equations are integrated backward in time because the boundary conditions for (12) that satisfy (6) must be specified at the final time for the adjoint variables. Therefore an adjoint

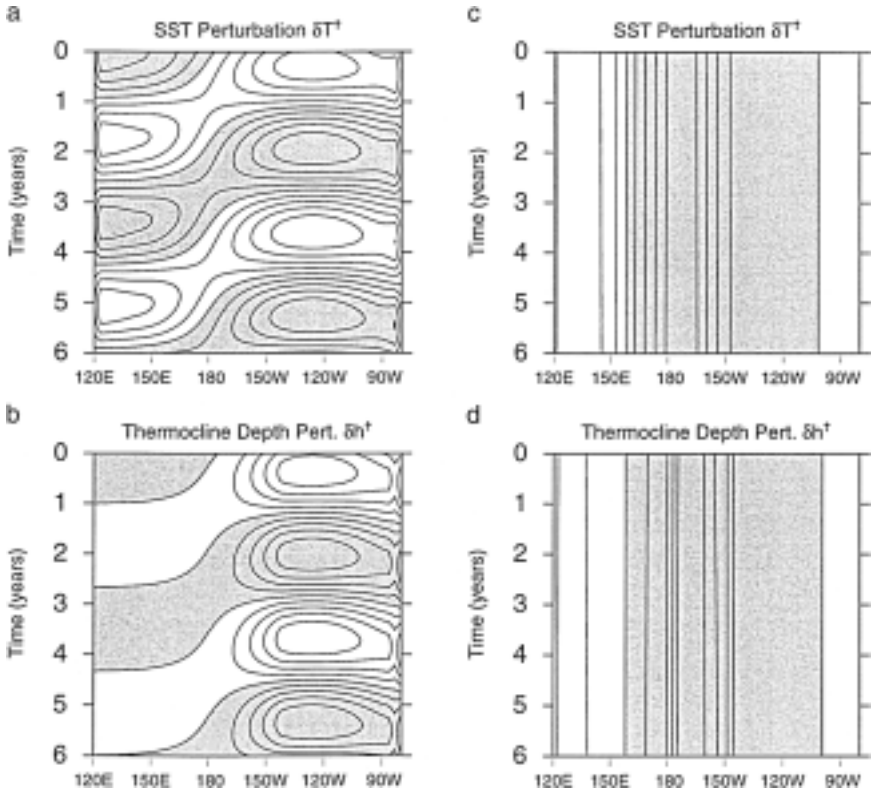

FIG. 8. Hovmöller diagrams of (a) the adjoint SST perturbation $\delta T^{\dagger}$ and (b) the adjoint thermocline depth perturbation $\delta h^{\dagger}$ along the equator for the gravest adjoint normal mode of the tangent linear coupled model when δDTF $\neq 0$ and δLH $= 0$. Hovmöller diagrams of (c) $\delta T^{\dagger}$ and (d) $\delta h^{\dagger}$ for the gravest adjoint normal mode when δDTF $= 0$ and δLH $\neq 0$ are also shown. The contour intervals are arbitrary. Shaded regions represent negative perturbations.

Kelvin wave propagates westward from a region where the mean thermocline depth is shallow and upwelling is strong (large α) to a region where the mean thermocline is deep and the upwelling weak (small α). Note that the interactions between the adjoint ocean and adjoint atmosphere are exactly those that are prohibited (i.e., deemed unimportant or unphysical) in the tangent linear coupled model leading to our ''one-way street analogy'' [e.g., δh directly changes δT in the tangent linear form of (11), while $\delta T^{\dagger}$ directly changes $\delta h^{\dagger}$ in the adjoint model]. Therefore as an adjoint Kelvin wave moves westward it couples with the adjoint atmosphere and the adjoint coupled mode amplifies in the west due to δLH† (cf. Fig. 5) in much the same way as the coupled normal mode amplifies in the east due to δDTF. If δLH $= 0$, then one atmospheric heat source available to adjoint Kelvin waves in the west is removed and the adjoint normal mode relies more on the adjoint direct thermal heating for its structure as shown in Figs. 8a and 8b. If ''two-way streets'' were present, and if equatorial ocean Kelvin (planetary) waves could propagate westward (eastward) as well as eastward (westward), then the gravest coupled mode would tend to have SST maxima in the east and west, in both the tangent linear model and adjoint model, thus rendering the system more normal.

3) THE CASE WHEN δLH $= 0$ AND α IS UNIFORM

From the preceding arguments it would appear that the very different structures of the normal mode and adjoint normal mode in the full model (cf. Figs. 4 and 5) is due to nonnormality arising from the presence of two sources of atmospheric heating [one confined primarily to the east (δDTF) and one confined primarily to the west (δLH)], in conjunction with the nonnormal nature of the ocean circulation that supports equatorial Kelvin waves that can propagate only to the east. We can test this argument in the following way. Note that the SST dipole of the gravest normal mode is asymmetric and occupies a larger area than that of the gravest adjoint normal mode, which is more symmetric. These differences are most likely due to the asymmetry of δDTF and δLH about the central Pacific, and differences in their areal extent (i.e., δLH $\neq 0$ when mean SST ≥ 28°C, whereas δDTF $\neq 0$ when $\delta T \neq 0$). Therefore we would expect that if the two sources of atmospheric heating were similar to each other in strength

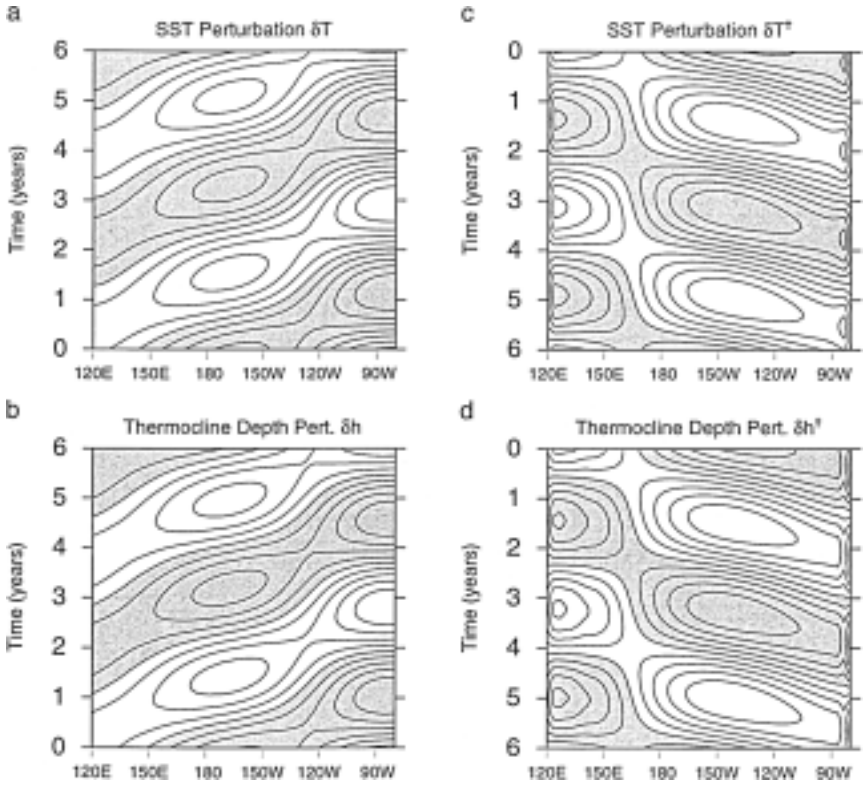

FIG. 9. Hovmöller diagrams of (a) δT and (b) δh along the equator for the gravest normal mode of the tangent linear coupled model when δDTF $\neq 0$, δLH $= 0$ and $\alpha = 2.5 \times 10^{-8}$°C m^{-1} s^{-1} at all longitudes. Hovmöller diagrams of (c) $\delta T^{\dagger}$ and (d) $\delta h^{\dagger}$ for the gravest adjoint normal mode for the case described in (a) and (b) are also shown. The contour intervals are arbitrary. Shaded regions represent negative perturbations.

and areal extent, then the SST dipoles of the gravest coupled normal mode and adjoint coupled normal mode would resemble mirror images of one another.

One way to make the heat sources in the east and west similar is to let δLH $= 0$ and assign a uniform value to α along the equator, which is equivalent to a flat basic-state thermocline and a spatially uniform rate of equatorial upwelling. In this case Kelvin waves in the tangent linear model couple as before with the atmosphere as they move eastward and grow. In the same way adjoint Kelvin waves in the adjoint model couple with the adjoint atmosphere as they move westward. The gravest coupled normal mode and adjoint coupled normal mode for the case when δDTF $\neq 0$, δLH $= 0$, and $\alpha = 2.5 \times 10^{-8}$°C m^{-1} s^{-1} at all longitudes are shown in Fig. 9. While the normal mode and adjoint mode are not exact mirror images of each other, they are more similar in this regard than the normal mode and adjoint mode of Figs. 4 and 5. Exact mirror images do not result because the nonnormal nature of the equatorial ocean waves renders ocean circulation fields and adjoint circulation fields that have very different two-dimensional structures due to the nature of the one-way streets discussed earlier.

b. *Variations in mode structure with α and dissipation*

The results of section 7a suggest that the spatial structure and oscillatory nature of ENSO in the autonomous coupled model are determined primarily by δDTF, while the structure of the adjoint ENSO mode (snapshots of which resemble the structure of intraseasonal surface heat flux perturbations) is determined by δLH. In this section we will examine the influence of nonnormality associated with ocean thermodynamics and dissipation on the mode structures.

Figure 10 shows the structure of the gravest normal mode and adjoint normal mode when δDTF $\neq 0$, δLH $\neq 0$, and $\alpha = 2.5 \times 10^{-8}$°C m^{-1} s^{-1} at all longitudes. Clearly the confinement of the adjoint normal mode SST signature to the west is not fundamentally altered by variations in α. Figure 11 shows similar results for the gravest normal mode and adjoint normal mode when the Newtonian cooling and Rayleigh friction coefficients in the model are reduced by a factor of 2. Other experiments have revealed that variations in the structure of the observed climatological fields of wind and humidity, that make up the coupled model basic state, do not alter the results and conclusions presented here.

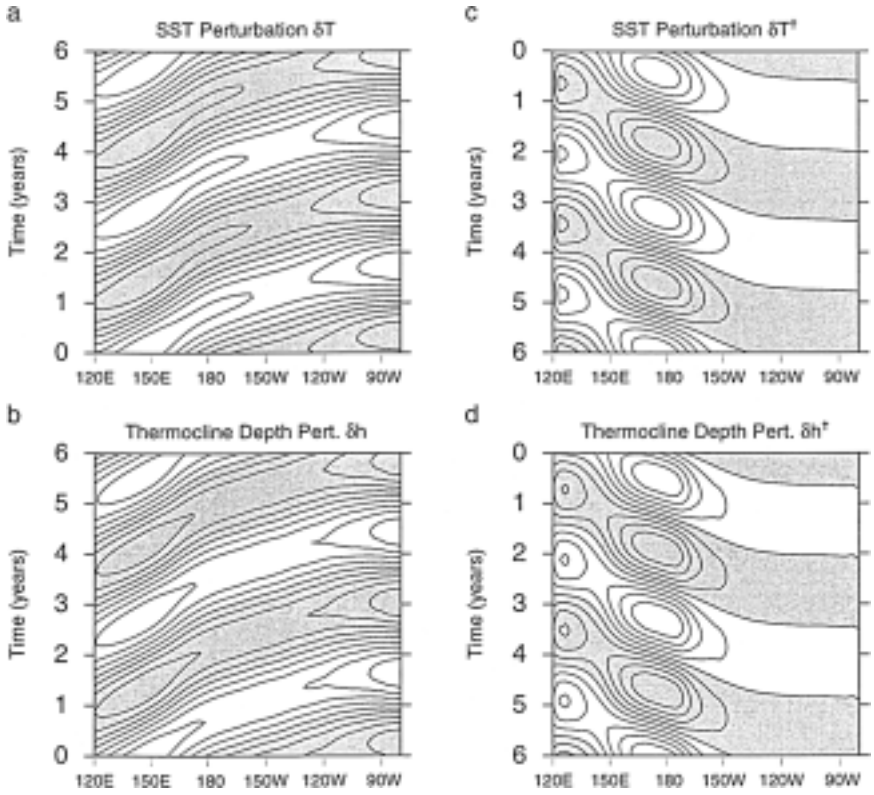

FIG. 10. Hovmöller diagrams of (a) δT and (b) δh along the equator for the gravest normal mode of the tangent linear coupled model when $\alpha = 2.5 \times 10^{-8}$°C m^{-1} s^{-1} at all longitudes. Hovmöller diagrams of (c) $\delta T^{\dagger}$ and (d) $\delta h^{\dagger}$ for the gravest adjoint normal mode for the case described in (a) in (b) are also shown. The contour intervals are arbitrary. Shaded regions represent negative perturbations.

c. The influence of zonal advection on SST

As noted in section 4, horizontal advection can influence the development of SST anomalies during ENSO episodes because of the sizeable surface current anomalies that develop in the ocean (Picaut et al. 1996). In the coupled model, the effects of zonal advection on SST can be parameterized by adding the terms $\overline{u}\partial T/\partial x + u\partial(\overline{T} + T)/\partial x$ to the right-hand side of (11), where $\overline{T}$ and $\overline{u}$ are the climatological mean SST and zonal velocity of the ocean mixed layer, respectively, and u is the mixed layer zonal velocity anomaly. In the tangent linear coupled model described by (12), zonal advection of SST introduces additional nonzero elements in the matrix $\mathbf{A}$, which change sign in the adjoint $\mathbf{A}^{\dagger}$. Therefore horizontal advection is another thermodynamic process in the upper ocean that influences the nonnormality of the coupled system.

When SST perturbations are controlled both by vertical displacements of the ocean thermocline and by zonal advection, the structure of the gravest normal mode is very similar to the ENSO mode of Fig. 4 (see also Kleeman 1993). The period of this mode increases with γ and eventually becomes nonoscillatory. Jin and Neelin (1993) discuss in detail the behavior of such coupled modes to changes in coupling strength. The spectrum of the normal mode eigenvalues is very similar to that shown in Figs. 3a and 3b.

The analyses of sections 6 and 7a were repeated for the case where both vertical movements of the thermocline and zonal advection influence SST. Figure 12 summarizes the results and shows Hovmöller diagrams of δT for the gravest normal mode and adjoint mode from the full tangent linear model,[1] when δDTF $\neq 0$ and δLH $= 0$, and when δDTF $= 0$ and δLH $\neq 0$ The normal mode spectra for the latter cases are similar to those shown in Figs. 3c–f. The conclusions of sections 6 and 7a are confirmed in this case also: the ENSO mode SST structure is confined to the east Pacific, the adjoint ENSO mode SST is confined to the west Pacific, and δLH and δDTF control the structure of these modes in the same way as when zonal advection is absent.

[1] When a seasonally varying basic state is considered, the period of the gravest normal mode is ~3–4 yr.

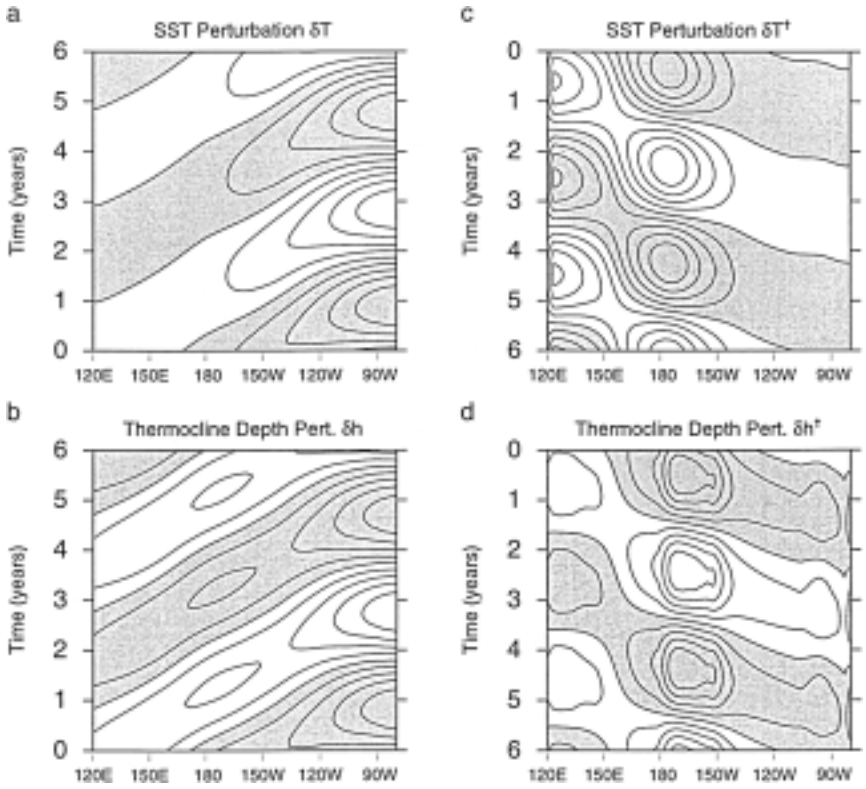

FIG. 11. Hovmöller diagrams of (a) δT and (b) δh along the equator for the gravest normal mode of the tangent linear coupled model when the Newton cooling and Rayleigh friction coefficients are reduced by a factor of 2. Hovmöller diagrams of (c) $\delta T^{\dagger}$ and (d) $\delta h^{\dagger}$ for the gravest adjoint normal mode for the case described in (a) and (b). The contour intervals are arbitrary. Shaded regions represent negative perturbations.

8. Discussion

Intraseasonal variability in the tropical west Pacific produces large-scale circulation anomalies that are associated with dipole or tripole convective anomalies and surface heat flux anomalies. This is because if atmospheric convection is enhanced in one region, the increase in ascending motion there must be balanced by an increase in descending motion to the east and/or west, which will tend to reduce convective activity in these regions. This is nicely illustrated in a recent study by Wheeler and Kiladis (1999), who performed a detailed analysis of outgoing longwave radiation in the Tropics to reveal how intraseasonal variability is partitioned between different convectively modified equatorial wave modes in the atmosphere. Figure 13 from Wheeler and Kiladis (1999) shows Hovmöller diagrams of OLR due to various equatorial modes of variability during the period September 1992–March 1993, which spans the TOGA Comprehensive Ocean–Atmosphere Research Experiment (COARE). All modes of variability produce dipole and tripole convective anomalies, but the mode that matches best the horizontal length scale of a snapshot of the adjoint ENSO mode SST dipole of Fig. 5a is the MJO of Fig. 13a.

Let us suppose for a moment that the real world behaves like the coupled model, then Fig. 13a and Fig. 5a suggest that surface heat flux perturbations associated with the MJO could act as effective precursors for ENSO because they project onto the SST structure of the adjoint ENSO mode. The difference in frequency between the MJO (~30–60 days) and the adjoint ENSO mode (~3 yr) is not of concern (see MK99) since the duration of individual MJO events is usually long enough to produce a significant oceanic response; it is the similarity between the spatial structure of the MJO surface heat flux and the adjoint ENSO mode SST that is most important. Observational studies have shown that the ability of the MJO to amplify in the west Pacific and produce a dipole surface heat flux perturbation depends critically on convective latent heating, δLH, and as shown in section 7 it is also δLH in the west that critically determines the SST structure of the adjoint ENSO mode. We have also demonstrated in section 7 that the ENSO mode that results from a perturbation in the form of a snapshot of the adjoint ENSO mode is controlled primarily by δDTF in the east; δLH has very little effect on the ENSO mode. It would appear therefore that ENSO as we know it could exist in the absence of δLH, but MJO could not. On the otherhand, MJO as we know it could exist in the absence of δDTF, but

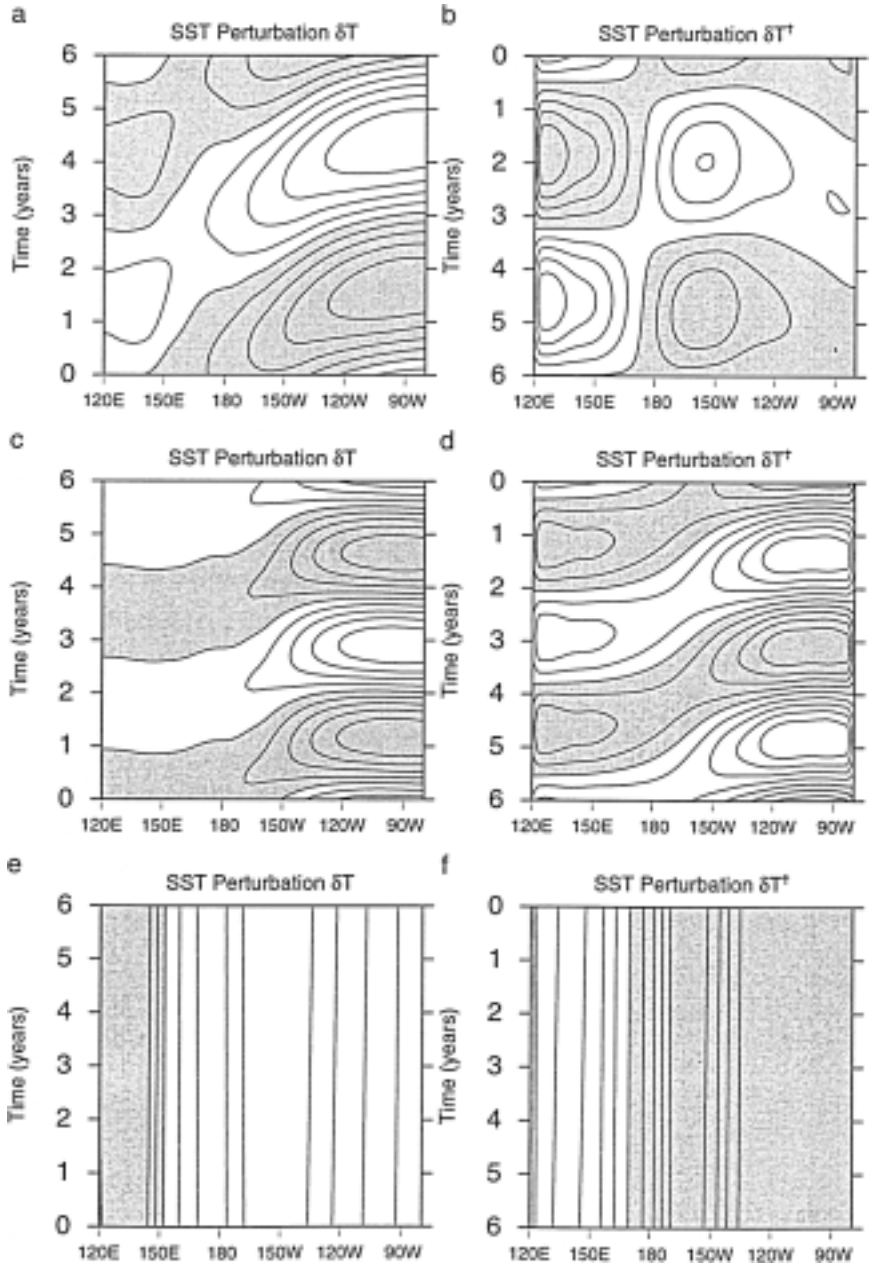

FIG. 12. Hovmöller diagrams of δT for the gravest normal mode and $\delta T^{\dagger}$ for the gravest adjoint normal mode when both thermocline displacements and zonal advection influence SST, for (a, b) the full tangent linear coupled model, (c, d) the case when $\delta\text{DTF} \neq 0$ and $\delta\text{LH} = 0$, and (e, f) the case when $\delta\text{DTF} = 0$ and $\delta\text{LH} \neq 0$.

ENSO could not. It is therefore pertinent to ask how δDTF and δLH are related. To understand this, consider the west Pacific warm pool, which drives the ascending branch of the Walker circulation. An important component of the Walker circulation is the easterly trade winds of the Pacific, which act to confine the warm pool to the west. The latent heat source δLH depends on the size of the warm pool, which in turn is controlled by the strength of the easterly trade winds. The direct thermal forcing δDTF is due to SST anomalies that develop in response to ocean upwelling in the east and central Pacific, and the upwelling strength depends on the strength of the easterly trade winds. Strong (weak) easterly trade winds therefore create conditions that are favorable for large (small) δDTF and small (large) δLH. Thus δDTF and δLH are related to each other, and are inextricably linked to the Walker circulation via the Pacific trade winds.

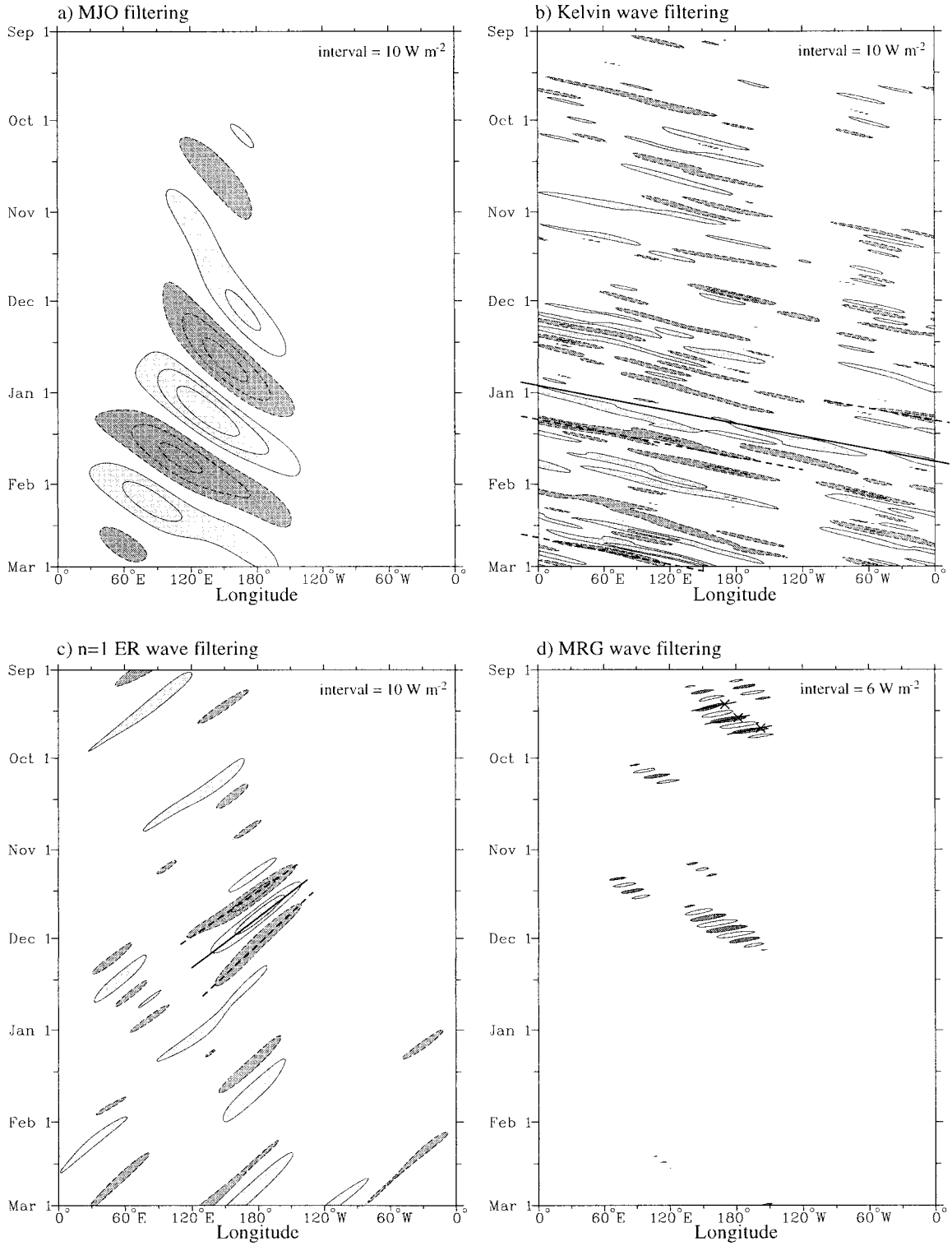

FIG. 13. (a) Hovmöller diagrams of the OLR anomalies associated with the MJO, averaged between 10°S and 2.5°N for the period 1 Sep 1992–1 Mar 1993. Light shading indicates positive anomalies and dark shading negative anomalies. (b) Same as (a) except for Kelvin waves. (c) Same as (a) except for the lowest order Rossby wave. (d) Same as (a) except for the mixed Rossby–gravity wave (from Wheeler and Kiladis 1999).

In section 3 we posed the question: is it merely coincidental that the structure of the MJO surface heat flux is similar to the SST structure of the optimal excitation of ENSO (i.e., the adjoint ENSO mode)? The answer to this question would appear to be no given (a) the dependence of ENSO on δDTF, (b) the dependence of the adjoint ENSO structure on δLH, (c) the dependence of the ability of the MJO to amplify on δLH, and (d) the link between δDTF, δLH, and the Walker circulation. The ability of the MJO to effectively initiate ENSO episodes therefore appears to be due to a combination of the large-scale Walker circulation over the Pacific, which controls both phenomena, and the fact that equatorial Kelvin waves propagate only to the east and long planetary waves propagate only to the west. Both of these factors are responsible for the nonnormal nature of the coupled ocean–atmosphere system in the tropical Pacific. This is an idea that deserves further study using other coupled models and observations of the coupled system.

9. Summary and conclusions

Recent modeling and stochastic–dynamic prediction efforts suggest that ENSO episodes may be stochastically forced by higher-frequency transient activity in the atmosphere and ocean. There is some circumstantial observational evidence to support this idea, particularly in relation to the 1997–98 El Niño event. It is argued that intraseasonal variability in the tropical west Pacific can act as an effective noise forcing mechanism for ENSO. The structure of the perturbations and disturbances that develop as a result of intraseasonal variability, however, have structures that are quite different to ENSO. Nevertheless they can act as effective precursors for ENSO episodes because of the nonnormal character of the coupled ocean–atmosphere system. These ideas have been advanced in the literature by a number of investigators (including the authors). Nonnormality though is somewhat of a mathematical concept, and previous studies have offered little insight into the physical attributes of the system that account for its nonnormality. This has been the primary focus of this study.

To examine the physics of nonnormality, we have used an intermediate coupled ocean–atmosphere model that we believe captures some important aspects of nature as they relate to ENSO. The relatively high predictive skill of the coupled model (Kleeman et al. 1995) offers some evidence that this is a reasonable assumption. Based on the physics inherent in the coupled model, we have identified five factors that contribute to the nonnormality of the coupled ocean–atmosphere system in the Tropics. They are (i) nonsolar atmospheric heating due to changes in SST, (ii) the dissimilarity between the equatorial ocean wave reflection process at eastern and western boundaries, (iii) ocean surface wind stress, (iv) upper-ocean thermodynamics, and (v) dissipation. This list is not exhaustive, and it is likely that there are other factors in nature, such as atmosphere–biosphere interactions, that also contribute to the nonnormality of the climate system. However, of the five factors identified in the coupled model used here, a combination of (i) and (ii) appears to account for the ability of perturbations associated with intraseasonal variability to act as effective precusors for ENSO episodes. The role of (iii) and (iv) is to couple the ocean and atmosphere, and as we have shown the inclusion of additional physics in (iv), such as zonal advection, does not affect our conclusions. Dissipation is clearly important in any dynamical system, but its effects on the nonnormality of the coupled system appear to be inert.

The nonsolar atmospheric heating related directly to SST is composed of two parts: one confined to the west Pacific due to deep atmospheric convection over the warm pool, and the other confined to the east due to ocean upwelling and a shallow thermocline. Both of these heat sources are intimately linked with the Walker circulation and its relationship with the warm pool.

The analyses presented here have been confined to autonomous systems, although the analysis of nonautonomous systems is straightforward in the framework of section 2. Moore and Kleeman (1996, 1997a,b, 1999) have shown that the growth of optimal perturbations and stochastically induced perturbations in a nonautonomous coupled model depends on the time evolution of the basic state and seasonal cycle, but their calculations show that the basic conclusions presented here are unaltered in a nonautonomous system.

The ideas presented here are based on the analysis of an intermediate coupled model. However, the factors that contribute to nonnormality identified as (i)–(v) above will also influence the nonnormality of all coupled models, and the real coupled system. As we have demonstrated, however, the structures of the gravest coupled adjoint normal mode, the optimal perturbations, and stochastic optimals may vary from model-to-model depending on the way that atmospheric heating is parameterized, and on the relative importance of the different heating regions. To date the optimal perturbations of three different coupled models with quite different parameterizations of atmospheric heating have been computed, and differences between them are apparent (see Moore and Kleeman 1996; Chen et al. 1997; Xue et al. 1997a,b; Yun 1997). The ideas presented in this paper therefore deserve further investigation in other coupled models to determine how robust the conclusions are that we present here as they apply to nature.

Finally, we end on a theoretical note by recalling that the adjoint ENSO mode is the optimal excitation for the ENSO mode in the tangent linear coupled system. However, the biorthogonality relation (7) also shows that the ENSO mode will be the optimal excitation for the adjoint ENSO mode in the adjoint coupled system. By using ideas developed in nonlinear systems theory and theoretical physics, it may be possible to use relationships between $\mathbf{R}$ and $\mathbf{R}^{\mathrm{T}}$ to explain the influence that

ENSO may have on intraseasonal variability. This will be the subject of further study.

Acknowledgments. This work was supported by a grant from the NOAA Office of Global Programs (NA76GP0478). We are indebted to Prof. Dan Sorensen and coworkers at Rice University for their outstanding efforts in developing the ARPACK software, which was used for all of the normal mode calculations described in this paper.

REFERENCES

Blanke, B., J. D. Neelin, and D. Gutzler, 1997: Estimating the effect of stochastic windstress forcing on ENSO irregularity. *J. Climate,* **10,** 1473–1486.

Chen, Y.-Q., D. S. Battisti, T. N. Palmer, J. Barsugli, and E. S. Sarachick, 1997: A study of the predictability of tropical Pacific SST in a coupled atmosphere/ocean model using singular vector analysis: The role of the annual cycle and the ENSO cycle. *Mon. Wea. Rev.,* **125,** 831–845.

Eckert, C., and M. Latif, 1997: Predictability of a stochastically forced hybrid coupled model of El-Niño. *J. Climate,* **10,** 1488–1504.

Farrell, B. F., 1989: Optimal excitation of baroclinic waves. *J. Atmos. Sci.,* **46,** 1193–1206.

——, and P. J. Ioannou, 1993: Stochastic forcing of the linearized Navier–Stokes equations. *Phys. Fluids,* **5A,** 2600–2609.

——, and ——, 1996a: Generalized stability theory. Part I: Autonomous operators. *J. Atmos. Sci.,* **53,** 2025–2040.

——, and ——, 1996b: Generalized stability theory. Part II: Nonautonomous operators. *J. Atmos. Sci.,* **53,** 2041–2053.

Graham, N., and T. P. Barnett, 1987: Observations of sea surface temperature and convection over tropical oceans. *Science,* **238,** 657–659.

Hirst, A. C, 1986: Unstable and damped equatorial modes in simple coupled ocean–atmosphere models. *J. Atmos. Sci.,* **43,** 606–630.

Jin, F.-F., and J. D. Neelin, 1993: Modes of interannual tropical ocean–atmosphere interaction—A unified view. Part I: Numerical results. *J. Atmos. Sci.,* **50,** 3477–3503.

Kestin, T. S., D. J. Karoly, J.-I. Yano, and N. A. Raynor, 1997: Time-frequency variability of ENSO and stochastic simulations. *J. Climate,* **11,** 2258–2272.

Kleeman, R., 1989: A modelling study of the effects of the Andean mountains of the summertime circulation of tropical South America. *J. Atmos. Sci.,* **46,** 3344–3362.

——, 1991: A simple model of the atmospheric response to ENSO sea surface temperature anomalies. *J. Atmos. Sci.,* **48,** 3–18.

——, 1993: On the dependence of hindcast skill on ocean thermodynamics in a coupled ocean–atmosphere model. *J. Climate,* **6,** 2012–2033.

——, 1994: Forecasts of tropical Pacific SST using a low-order coupled ocean–atmosphere dynamical model. NOAA Experimental Long-Lead Forecast Bulletin (since June 1994), Washington, DC.

——, and A. M. Moore, 1997: A theory for the limitations of ENSO predictability due to stochastic atmospheric transients. *J. Atmos. Sci.,* **54,** 753–767.

——, and ——, 1999: New method for determining the reliability of dynamical ENSO predictions. *Mon. Wea. Rev.,* **127,** 694–705.

——, ——, and N. R. Smith, 1995: Assimilation of sub-surface thermal data into an intermediate tropical coupled ocean–atmosphere model. *Mon. Wea. Rev.,* **123,** 3103–3113.

Lanczos, C., 1961: *Linear Differential Operators.* Van Nostrand, 564 pp.

Lau, K.-M., 1985: Elements of a stochastic–dynamical theory of the long-term variability of the El Niño/Southern Oscillation. *J. Atmos. Sci.,* **42,** 1552–1558.

Moore, A. M., and R. Kleeman, 1996: The dynamics of error growth and predictability in a coupled model of ENSO. *Quart. J. Roy. Meteor. Soc.,* **122,** 1405–1446.

——, and ——, 1997a: The singular vectors of a coupled ocean–atmosphere model of ENSO. Part I: Thermodynamics, energetics and error growth. *Quart. J. Roy. Meteor. Soc.,* **123,** 953–981.

——, and ——, 1997b: The singular vectors of a coupled ocean–atmosphere model of ENSO. Part II: Sensitivity studies and dynamical significance. *Quart. J. Roy. Meteor. Soc.,* **123,** 983–1006.

——, and ——, 1998: Skill assessment for ENSO using ensemble prediction. *Quart. J. Roy. Meteor. Soc.,* **124,** 557–584.

——, and ——, 1999: Stochastic forcing of ENSO by the intraseasonal oscillation. *J. Climate,* **12,** 1199–1220.

Penland, C., 1996: A stochastic model of IndoPacific sea surface temperature anomalies. *Physica D,* **98,** 534–558.

——, and L. Matrasova, 1994: A balance condition for stochastic numerical models with application to El Niño Southern Oscillation. *J. Climate,* **7,** 1352–1372.

——, and P. D. Sardeshmukh, 1995: The optimal growth of tropical sea surface temperature anomalies. *J. Climate,* **8,** 1999–2024.

Picaut, J., M. Ioualalen, C. Menkes, T. Delcroix, and M. J. McPhaden, 1996: Mechanisms of the zonal displacements of the Pacific warm pool: Implications for ENSO. *Science,* **274,** 1486–1489.

Vallis, G. K., 1988: Conceptual models of El Niño and the Southern Oscillation. *J. Geophys. Res.,* **93,** 13 979–13 991.

Wheeler, M., and G. N. Kiladis, 1999: Convectively coupled equatorial waves: Analysis of clouds in the wavenumber–frequency domain. *J. Atmos. Sci.,* **56,** 374–399.

Xue, Y., M. A. Cane, and S. E. Zebiak, 1997a: Predictability of a coupled model of ENSO using singular vector analysis. Part I: Optimal growth in seasonal background and ENSO cycles. *Mon. Wea. Rev.,* **125,** 2043–2056.

——, ——, ——, and T. N. Palmer, 1997b: Predictability of a coupled model of ENSO using singular vector analysis. Part II: Optimal growth and forecast skill. *Mon. Wea. Rev.,* **125,** 2057–2073.

Yun, F., 1997: ENSO prediction and predictability in an intermediate coupled model. Ph.D. thesis, University of Oxford, United Kingdom, 257 pp. [Available from Dept. of Atmospheric, Oceanic, and Planetary Physics, University of Oxford, Parks Rd., Oxford OX1 3PU, United Kingdom.]